Study of the effect of ordered porosity and surface silanization on in vitro bioactivity of sol-gel-derived bioactive glasses

K. Aneb, Hassane Oudadesse, H. Khireddine, B. Lefeuvre, Odile Merdrignac-Conanec, F. Tessier, A. Lucas

Study of the effect of ordered porosity and surface silanization on *in vitro* bioactivity of sol-gel-derived bioactive glasses.

K. Aneb[a,b*], H. Oudadesse[a], H. Khireddine[b], B. Lefeuvre[a], O. Merdrignac-Conanec[a], F. Tessier[a], A. Lucas[a*].

[a]Univ Rennes, CNRS, ISCR-UMR 6226, F-35000, Rennes, France.

[b]Laboratoire de Génie de l'Environnement, Département de Génie des Procédés, Faculté de Technologie, Université de Bejaia, Algérie.

Abstract

The modification of porosity and surface silanization are efficient methods to improve physicochemical and biological properties of bioactive glass. For sol-gel-derived glasses, the use of surfactant in the synthesis medium allows to pattern porosity and may significantly impact their *in vitro* bioactivity. Additionally, surface functionalization by silanization may be a key method for grafting drugs or biomolecules to the glass surface. In this work, we realized a comparative study of the effect of porosity modification and surface silanization on *in vitro* bioactivity of sol-gel-derived bioactive glasses. The materials characterization by FTIR spectroscopy, XRD analysis, ICP-OES spectroscopy, and SEM-EDS, before and after soaking in SBF, showed that the ordered porosity increases significantly the kinetics of hydroxyl-carbonate apatite formation and induces a control of the mineralization at the glass surface. The results show also that the glass remains bioactive after silanization. The present work shows that porosity structuring both improves the *in vitro* bioactivity of our glass and increases the silanization rate of the glass surface.

Key-words: Bioactive glass, Sol-Gel, Silanization, Mesoporous, Bioactivity, Controlled mineralization.

1. Introduction

The first bioactive glass, named 45S5, was synthesized by L. Hench in the early 1970s [1-4]. Since then, bioactive glass has continued to be of interest to researchers for its use as a biomaterial for hard tissues. Its bioactivity allows the creation of bonds with living bone tissue

[*]Corresponding author.
Address: Équipe Verres et Céramiques, UMR 6226 CNRS, Université de Rennes 1, Institut des Sciences Chimiques de Rennes, Campus de Beaulieu, Bâtiment 10 B, Avenue du Général Leclerc, 35042 Rennes Cedex, France.
Tel/fax: +33 (0) 223236745.
E-mail addresses: anebkhalil89@gmail.com (K. Aneb), anita.lucas@univ-rennes1.fr (A. Lucas).

[5-9]. Many studies have been carried out to understand the physicochemical and biological behavior of bioactive glasses. Several parameters could influence the reactivity of the glass, including the synthesis method [10-15],textural features such as porosity structure and pore size [14-20], and the composition by incorporating elements of a physicochemical or biological interest [21-25].Yan et *al.* are the first research team that developed mesoporous bioactive glass with ordered porosity [26], this property results in an increased specific surface area and a well-defined porous structure in terms of shape and diameter, this impacts positively the bioactivity of the bioactive glass [27]. Since the bioactive glass is intended to be implanted in a bone site, it may play another role than just a bone filler. Adding therapeutic molecules can confer the glass an additional biological property such as increasing bone regeneration and/or antibacterial activity [28,29]. Surface silanization is one of the most widely used methods that allow the association between glass and different organic molecules [30]. This method consists in grafting to the surface of the glass a silane coupling agent with terminal functional groups [31].These groups will allow a chemical bond with one or more well-defined organic molecules. Nevertheless, for this approach to be successful in the purpose of bone implantation, the glass must remain bioactive after surface silanization. In this work, sol-gel derived glasses named92S6 and 92S6 P123 with wt% composition: (84.82% SiO_2 – 10.14 % CaO – 5.04 % P_2O_5) were synthesized and studied [16-19]. In a previous work, a comparative study of the synthesis of bioactive glass with an ionic surfactant (CTAB) and with a non-ionic surfactant (P123) was realized to highlight the effect of the chemical nature of the surfactant on glass physicochemical properties [18]. It was showed that, for the tested conditions, the presence of non-ionic surfactant P123 in the glass synthesis medium led to a hexagonal ordered mesoporosity. Conversely, the use of ionic surfactant CTAB did not allow to obtain the ordered mesoporosity [18]. Even if the non-ionic surfactant did not allow to order porosity, its presence might influence the textural glass property. In the present work, we synthesized a bioactive glass in presence of the non-ionic surfactant P123 and in strictly the same conditions, except the presence of a surfactant, its unordered counterpart synthesized without any surfactant. We then studied the effect of the ordered porosity induced by the presence in the synthesis medium of the non-ionic surfactant P123 both on porosity and bioactivity features. In addition, we studied the influence of functionalization by silanizationon the bioactivity features for the two glasses.

2. Materials and methods

2.1. Glass synthesis reactants

The different reagents for the glass synthesis are summarized in Table I. The pluronic P123 (Aldrich, France) was used as a surfactant for the synthesis of 92S6 with structured porosity named 92S6 P123 (see section below).

Table I. Reagents used for glass synthesis.

	Silica source	**Calcium source**	**Phosphorous source**	**Non-ionic surfactant**

Reagent	Tetraethyl orthosilicate (TEOS)	Calcium nitrate tetrahydrate ($Ca(NO_3)_2$, $4H_2O$)	Triethyl phosphate (TEP)	Pluronic P123
Supplier	Sigma-Aldrich	Fluka	Sigma-Aldrich	Sigma-Aldrich
Purity	98%	99%	99.8%	-

2.2. Preparation of bioactive glass samples

The bioactive glasses named 92S6 and 92S6 P123 were synthesized according to a procedure described elsewhere [16-19]. The 92S6 P123 is the notation which refers to the 92S6 glass synthesis in presence of the surfactant pluronic P123.

Surface silanization of the bioactive glasses

The two glasses were silanized with 3-aminopropyltriethoxysilane (APTES, 98%, Alfa-Aesar) as follows: glasses were dehydrated by a heat treatment at 200°C under vacuum and then refluxed with 20.10^{-3}mol of APTES per gram of glass in dehydrated toluene (20 mL/g of glass) for 24h at 120 °C under Argon. The obtained product was centrifugated and rinsed 3 times with a mixture of diethyl ether and dichloromethane (1:1) and finally dried at 100°C during 12h in air.

The Table II summarizes the four materials to be studied with their notations.

Table II. The materials studied and their notations.

Material	**Notation**
Non-silanized 92S6	92S6
Silanized 92S6	92S6 Sil
Non-silanized 92S6 P123	92S6 P123
Silanized 92S6 P123	92S6 P123 Sil

2.3. Glass characterization before and after silanization

Specific surface area and porosity features were analyzed at 77K using Nitrogen adsorption isotherms by a Gemini VII volumetric adsorption analyzer (Micromeritics, USA). Prior to measurements, the samples were outgassed during one night at ambient temperature in a VacPrep 061 degas system.

Specific surface areas were derived from the isotherms using the BET method and a set of 10 experimental points of the linear range of the BET plot ($0.05<P/P_0<0.3$).

The ordered porosity in 92S6 P123 was assessed by transmission electronic microscopy using a JEOL JEM 2100 LaB6 microscope operating at 200 KV. The images were obtained in a bright field using a high resolution Gatan US1000 camera, and an Orius 200D camera. The samples 92S6 and 92S6 P123 Sil were also analyzed for comparison.

The silane coupling agent contains an amine group. The nitrogen related to this functional group was quantified to determine the degree of silanization. The analysis was performed using inert gas fusion elemental analysis apparatus LECO TC 600 (LECO, USA). Nitrogen was measured as N_2 by thermal conductivity and oxygen as CO_2 by infrared detection. The apparatus was calibrated using LECO standards. Each analysis was done in triplicate. The mean weight percentage of nitrogen in glass and standard deviation were then calculated.

2.4. In vitro bioactivity test

To evaluate the *in vitro* bioactivity, each glass was soaked in a simulated body fluid (SBF). This solution which presents an ionic composition close to the human plasma (Table III) was synthesized in accordance to Kokubo procedure [32,33]. 25 mg of each of the four materials were immersed in 50 mL of SBF. The suspensions (glass in SBF) were placed in an incubator set at 37 °C with a rotation speed of 60 rpm for different soaking times {1, 5, 10 and 15 days}. The procedure was realized in triplicate.

Table III. Ionic composition of SBF compared to human blood plasma.

Ions	Na^+	K^+	Ca^{2+}	Mg^{2+}	HCO_3^-	Cl^-	HPO_4^{2-}
Plasma (mM)	142	5	2.5	1.5	27	103.8	1
SBF (mM)	142	5	2.5	1.5	4.2	148	1

2.5. Glass surface characterization before and after soaking in SBF

The glasses surface changes were characterized by FTIR spectroscopy, XRD analysis, and SEM-EDS before and after immersion in SBF. To quantify the ionic exchange between theglasses and SBF over time, the supernatant of SBF was collected and analyzed by ICP-OES after each soaking time.

2.5.1. XRD analysis

X-ray diffraction (XRD) patterns were recorded at room temperature in 10°-60° 2θ range with a step size of 0.0261° and an effective scan time per step of 300 s using a PANalytical X'Pert Pro diffractometer (Cu-L2,L3 radiation, λ = 1.5418 Å, 40 kV,40 mA, PIXcel 1D detector). Data collector and HighScore Plus programs were used, respectively, for recording and

analysis of the patterns. The purity of all the prepared powders was systematically checked by XRD.

2.5.2. FTIR spectroscopy

The FTIR spectroscopy was carried out at room temperature on KBr pellets containing the sample using a Alpha Bruker spectrometer between 4000 cm^{-1} and 400 cm^{-1} in transmittance mode with a resolution of 1 cm^{-1}.

2.5.3. SEM-EDS

Scanning electron microscopy coupled to Energy dispersive X-ray spectroscopy (SEM-EDS) was performed by a JEOL JSM 7100 F EDS EBSD (Oxford instrument) to examine the changes of the glasses surface before and after the different soaking times.

2.5.4. ICP-OES

The evolution of the elemental composition (Ca, Si, P) of the SBF after glass soaking was investigated by ICP-OES analysis preformed on SBF supernatant for each soaking time. The analysis was performed by Thermo Scientific iCAP 7000 series ICP-AES spectrometer.

3. Results and discussion

3.1. Porosity features

TEM micrographs and Fourier transform (FT) patterns show for 92S6 (Figure 1A) an unordered porosity and irregular pore distribution. Whereas, for the 92S6 P123 (Figure 1B) the results show an ordered porosity organized in channels gathered in a hexagonal shape. These results are consistent with those obtained by Letaïef *et al.* [18]. For the 92S6 P123 Sil (Figure 1.C), the image and FT patterns reveal that the ordered porosity is preserved after the glass surface silanization.

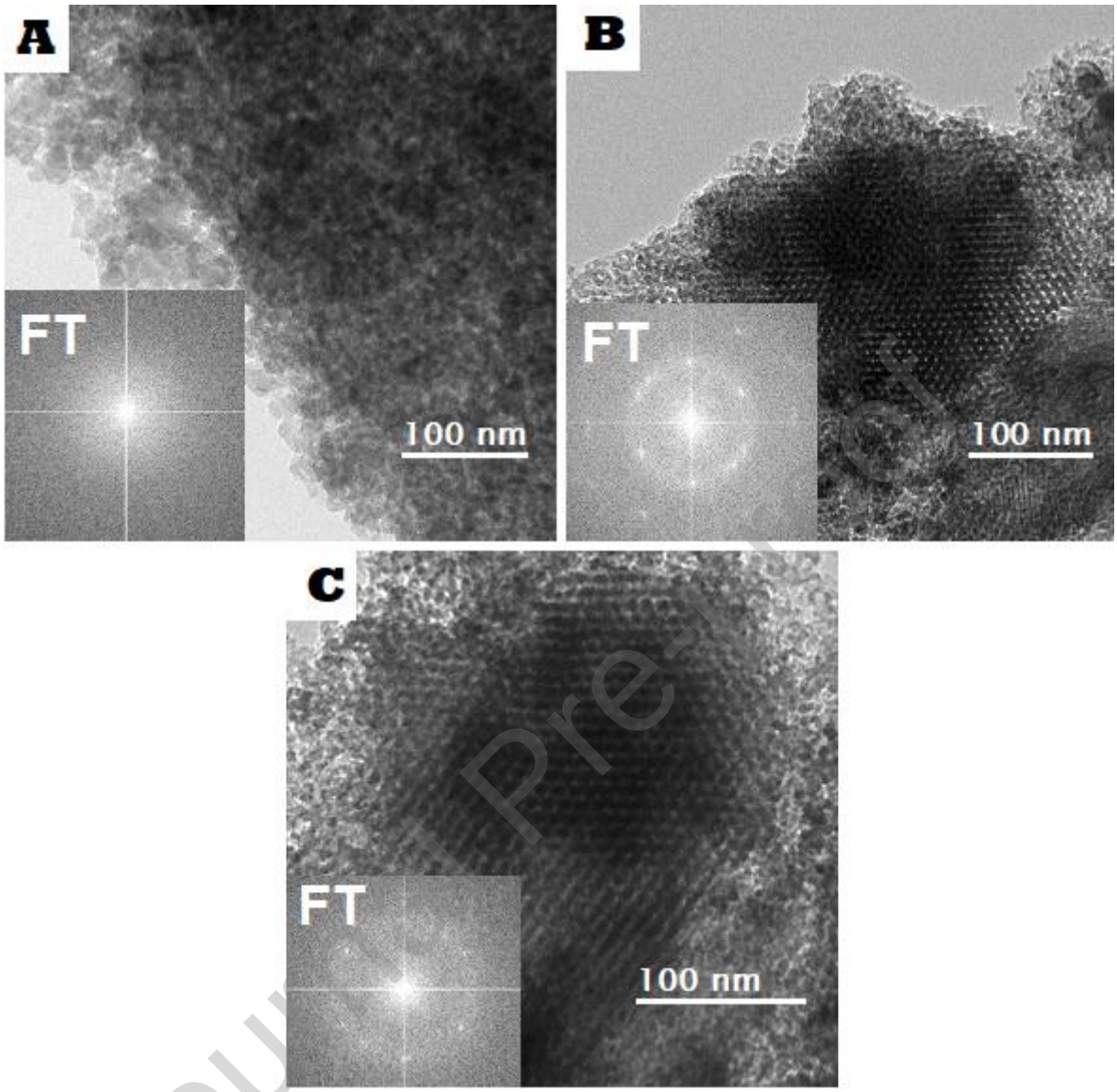

Figure 1. TEM micrographs for 92S6 (A), 92S6 P123 (B) and 92S6 P123 Sil (C) before soaking in SBF.

Specific surface area, total pore volume and BJH desorption average pore diameter for the different glasses are presented in Table IV. Results show greater specific surface area and average pore diameter for the glass presenting structured porosity (92S6 P123) than the glass presenting non-structured porosity (92S6). Results indicate also that the silanization decreased the specific surface area, probably because of the smoothing of the surface during the silanization process in solution. The pore diameters are smaller for silanized glasses due to the obstruction created by the carbon chains of the silane coupling agent (APTES) grafted at the pore surface [34]. However, the nitrogen adsorption and desorption isotherms (non-presented here) were not modified by the silanization process, which is consistent with an absence of modification of the main porosity features.

Table IV. Specific surface area (S_{BET}), total pore volume (V_P) and BJH desorption average pore diameter (D_P) for different glasses

Glass	S_{BET} (m^2/g)	V_P (cm^3/g)	D_P (Å)
92S6	372	0.8	65
92S6 Sil	280	0.6	59
92S6 P123	392	1.2	119
92S6 P123 Sil	342	1.3	69

3.2. Nitrogen content analysis

The comparison of glasses nitrogen content is presented in Table V. The increase of nitrogen content after silanization is consistent with the grafting of the silane coupling agent at the glass surface. Results indicate that the glass with structured porosity has a greater degree of silanization than the glass with non-structured porosity. Glass with structured porosity exhibits a lower dispersion in pore diameter than unstructured glass. This allows a regular and easier penetration of the APTES in the glass matrix, and then a greater grafting rate.

Table V. Nitrogen weight content for the different glasses.

Glass	Wt N (%) ± SD
92S6	0.34 ± 0.06
92S6 Sil	1.25± 0.03
92S6 P123	0.23 ± 0.06
92S6 P123 Sil	1.56± 0.11

3.3. XRD analysis

After soaking in SBF, the XRD patterns, for both glasses 92S6 (Figure 2.A) and 92S6 Sil (Figure 2.B), show an appearance of a small peak at 29.4°after 1 day of immersion. This peak is assigned to the calcite formed from day 1 of immersion. The calcite precipitation is related to the high concentration of Ca that was released in SBF solution from the glass matrix in the first hours of immersion. Indeed, the released calcium ions combine with carbonate ions CO_3^{2-} from SBF to form calcite which precipitates on the glass surface [35]. At day 5 and day 10, no changes were recorded. On day 15 of immersion, we recorded additional peaks that are assigned to (002), (211), (310), (222) and (004) reflection plans of hydroxyapatite (HA) crystals consistent with the presence of this crystallized phase at the glass surface [36,37]. The XRD patterns show, for 92S6 P123(Figure 2.C) and 92S6 P123 Sil (Figure 2.D), after 1 day of immersion, an appearance of peaks assigned to HA similar to those observed for 92S6 after 15 days of soaking in SBF. From day 5 up to day 15, we recorded an increase in the intensities of all recorded peaks for both 92S6 P123 and 92S6 P123 Sil. No peak assigned to calcite was recorded for 92S6 P123 and 92S6 P123 Sil throughout the whole soaking time.

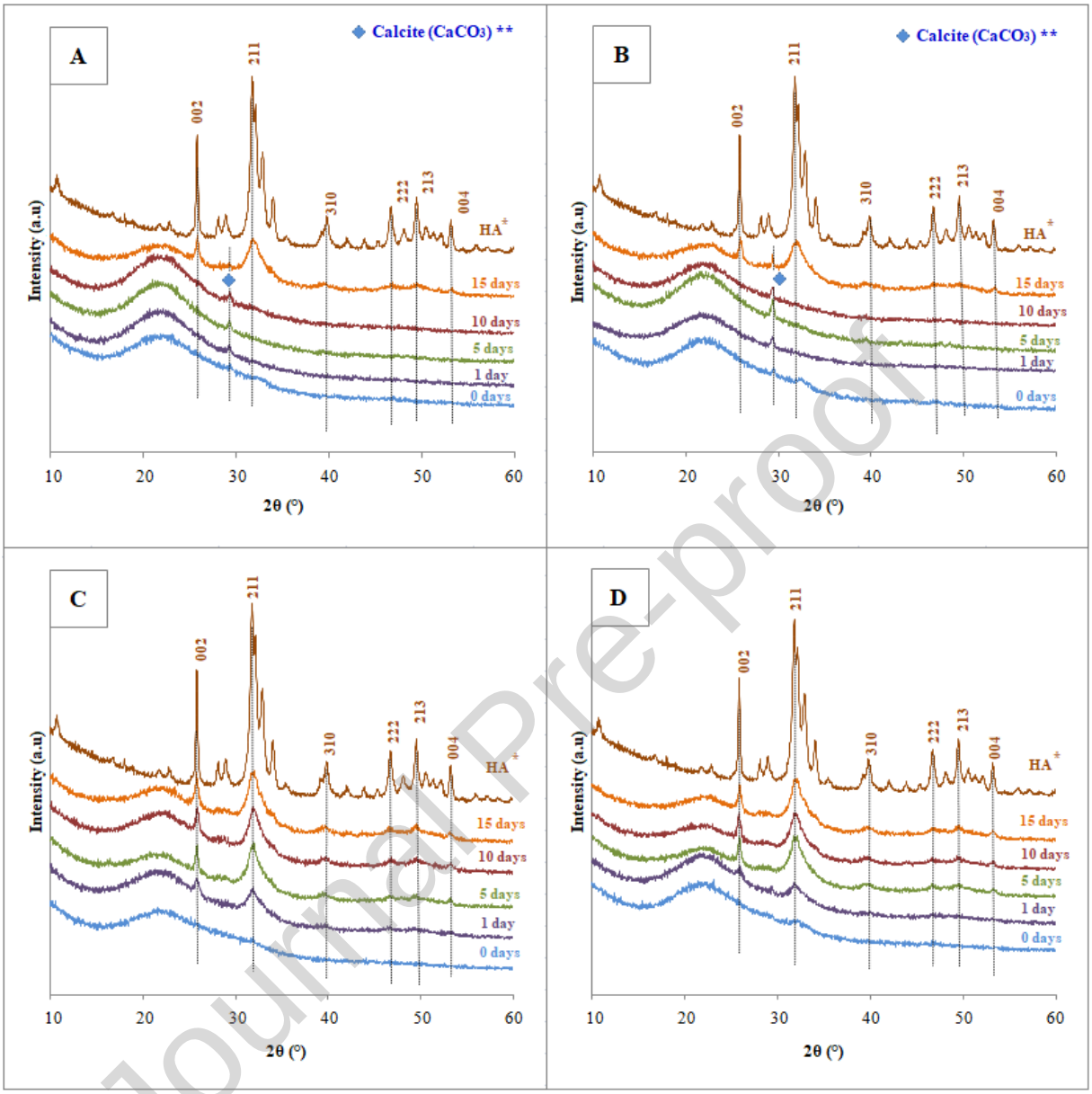

Figure 2. XRD patterns of glass surfaces before and after immersion in SBF solution at different testing times. A: 92S6, B: 92S6 Sil, C: 92S6 P123, D: 92S6 P123 Sil.
*Calcium hydroxide phosphate, AR powder (Alfa Aesar, Zeppelinstraße 7, 76185 Karlsruhe, Cat. # 304288, Lot#1386600).
**ICDD# 01-086-2340.

3.4. FTIR spectroscopy

The FTIR spectra (Figure 3) show, for all glasses, after 1 day of immersion an appearance of a new small band at 878 $cm^{-1}$and a large band between 1400 $cm^{-1}$and 1500 cm^{-1}.These bands are assigned to carbonate group (CO_3^{2-}) [38,39]. The bands recorded at 472 cm^{-1}, 566 cm^{-1} , 603cm^{-1} , 964 cm^{-1} and the large band between 1000 and 1100 cm^{-1} that covers the regions at 1034 cm^{-1} and 1093 $cm^{-1}$are assigned to tetrahedral phosphate group (PO_4^{3-}) [40,41]. The

dual-band at 566 cm^{-1} and 603 cm^{-1}, which is a characteristic of crystalline calcium phosphate in hydroxyapatite [1][42-44] appears after 1 day of immersion for 92S6 P123 (Figure 3.C) and 92S6 P123 Sil (Figure 3.D) and only after 15 days of immersion for 92S6 (Figure 3.A) and 92S6 Sil (Figure 3.B). The carbonate group bands recorded on the first day of immersion are assigned to carbonate present in calcite for 92S6 and 92S6 Sil, and to carbonate present in hydroxyl-carbonate apatite for 92S6 P123 and 92S6 P123 Sil at this stage of immersion. These results are in good agreement with the recorded XRD patterns (Figure 2).

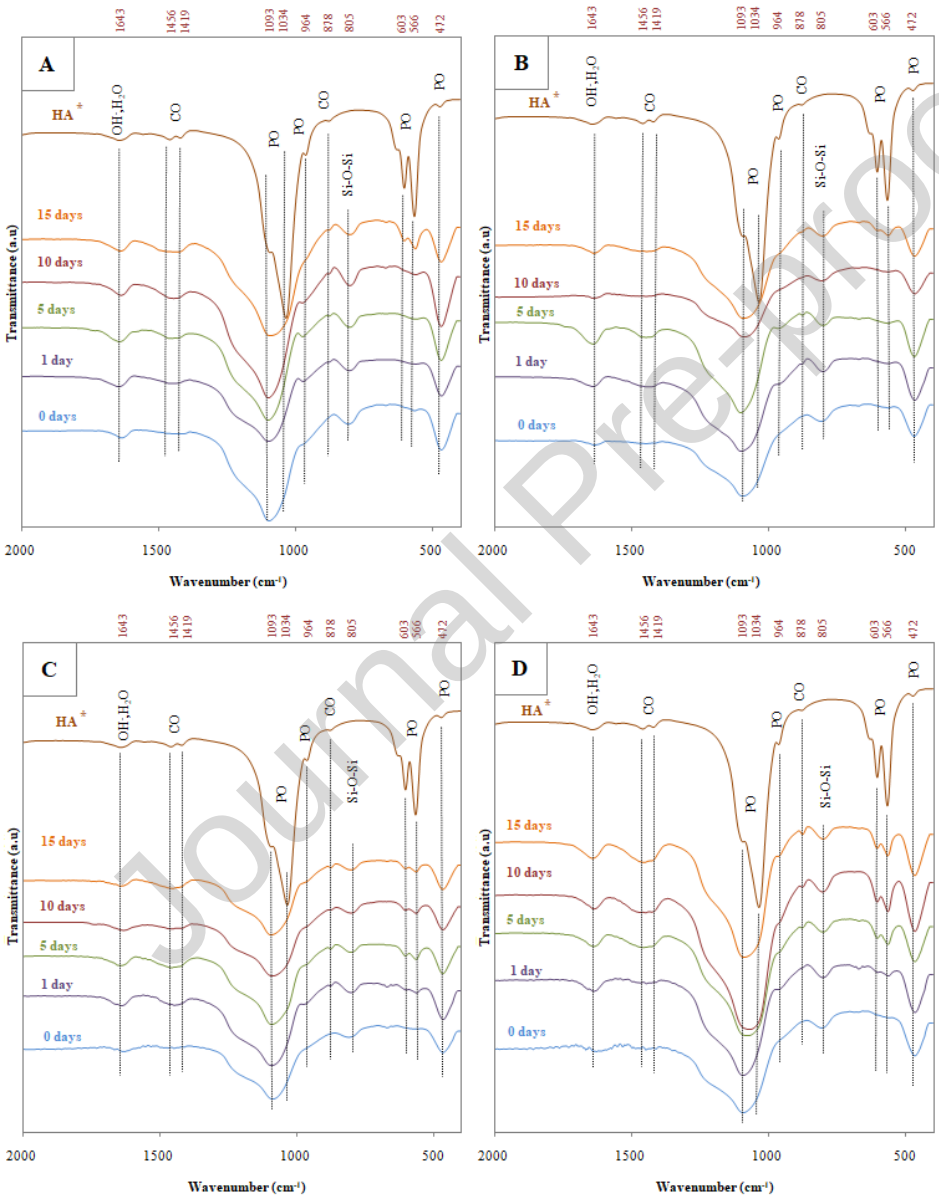

Figure 3. FTIR spectra of glass surfaces before and after immersion in SBF solution at different testing times. A: 92S6, B: 92S6 Sil, C: 92S6 P123, D: 92S6 P123 Sil.
*Calcium hydroxide phosphate, AR powder (Alfa Aesar, Zeppelinstraße 7, 76185 Karlsruhe, Cat. # 304288, Lot#1386600).

3.5. ICP-OES analysis of SBF

The ICP analysis of SBF solution after immersion of the glass 92S6 (Figure 4.A) shows at first an increase in Ca concentration after 1 day of immersion. From day 1 to day 5 we recorded a decrease in Ca concentration. From day 5 to day 10 Ca concentration remains more or less constant. From day 10 to day 15, Ca concentration decreases. The P concentration remains unchanged up to day 10, after this period up to 15 days of immersion, a decrease is recorded.

For 92S6 P123 (Figure 4.B), a slight decrease in Ca concentration is recorded on day 1. On day 5, the concentration decreases sharply, then the decrease continues slightly up to day 10. After that, the concentration remains practically unchanged up to day 15. The P concentration decreases slightly after day 1 of immersion, then the decrease continues sharply up to day 5, after that the concentration remains practically unchanged.

The Si concentration increases rapidly after the immersion, for both glasses, to reach a practically stationary phase without an important change at this stage.

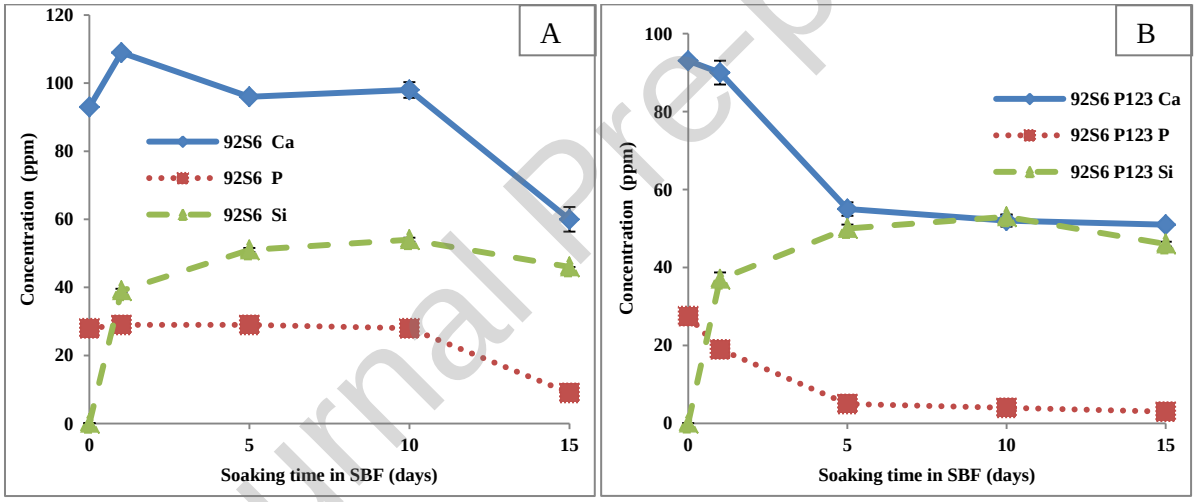

Figure 4. Evolution of (Ca), (P) and (Si) concentrations in SBF versus time soaking. A: 92S6, B: 92S6 P123.

The ICP-OES results for 92S6 versus 92S6-Sil and 92S6 P123 versus 92S6 P123-Sil (Figure 5) show that the evolution of the different ions concentration in SBF is the same for both silanized and non-silanized glass, this result is in a good agreement with the results obtain by FTIR-spectroscopy and XRD analysis which show no difference between the two variants of glass.

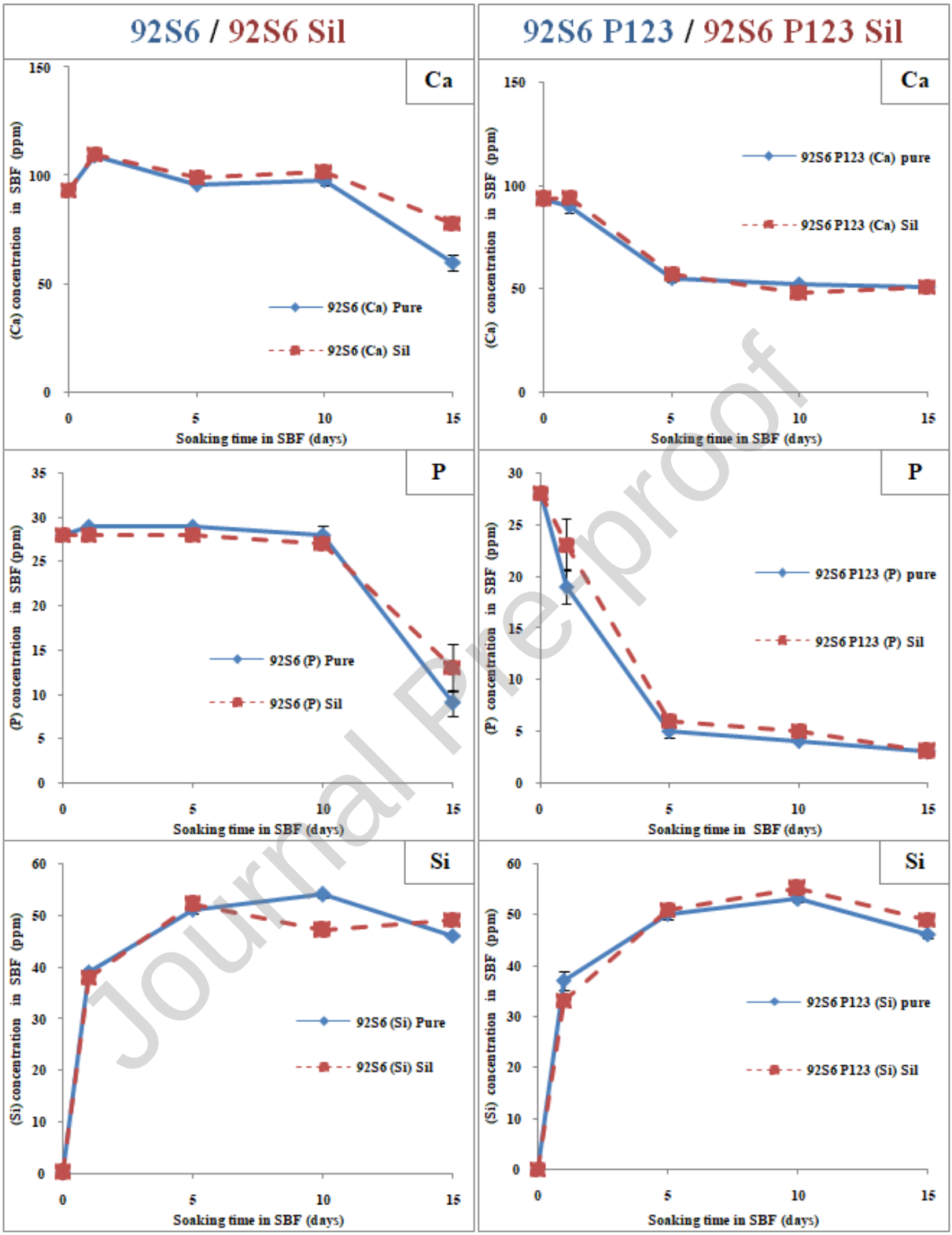

Figure 5. Evolution of (Ca), (P) and (Si) concentrations in SBF versus soaking time for silanized and non-silanized glasses.

3.6. SEM-EDS

The SEM micrographs before immersion for 92S6 (Figure 6.A), 92S6 Sil (Figure 6.D), 92S6 P123 (Figure 6.G) and 92S6 P123 Sil (Figure 6.J) show for all glasses an irregular surface with a granular appearance. The EDS results indicate, for all glasses, a surface very rich in silicon with small amounts of Ca and P, which is in good agreement with the elemental composition of all glasses before immersion in SBF. After 1 day of immersion, no change in surface aspect is recorded for 92S6 (Figure 6.B) and 92S6 Sil (Figure 6.E), whereas, small rods appeared on the surfaces of 92S6 P123 (Figure 6.H) and 92S6 P123 Sil (Figure 6.K). The EDS results show for 92S6 (Figures 6.B) and 92S6 Sil (Figure 6.E) the same results as before immersion. In contrary, for 92S6 P123 (Figure 6.H) and 92S6 P123 Sil (Figure 6.K), the EDS show a layer less rich in silicon and richer in Ca and P. By linking these results to FTIR spectra and XRD patterns, we conclude that the rods correspond to hydroxyl-carbonate apatite (HCA) crystals which was formed after 1 day of immersion on 92S6 P123 whether it's silanized or not. This indicate that no formation of calcium phosphate phase occurred at the glass surface after one day in contact with SBF, on both 92S6 and 92S6 Sil contrary to 92S6 P123 and 92S6 P123 Sil. These results are in accordance with ICP-OES results presented above. After 15 days of immersion, small rods, very similar to those recorded on 92S6 P123 and 92S6 P123 Sil from day 1 of immersion, appear on the surfaces of the 92S6 (Figure 6.C) and 92S6 Sil (Figure 6.F). For 92S6 P123 (Figures 6.I) and 92S6 P123 Sil (Figure 6.L), the same rods were recorded and became more abundant as compared to day 1.

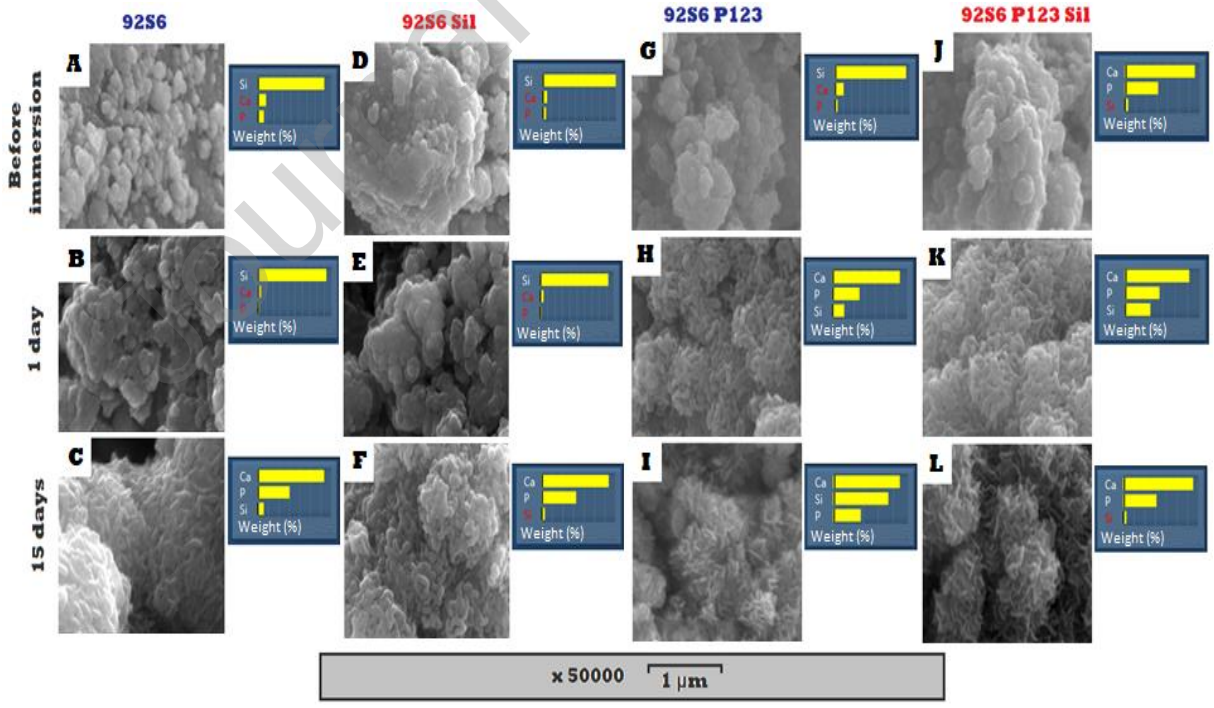

Figure 6. SEM micrographs and EDS spectra of 92S6 and 92S6 Sil surfaces before and after 1 day and 15 days of immersion in SBF.

3.7. Effect of ordered porosity on bioactivity

Figure 7 illustrates the different steps of the *in vitro* reactivity of bioactive glass in SBF described by L. Hench [5]. The increase in Ca^{2+} ion concentration in SBF is due to the cationic exchange between the glass surface and SBF: Ca^{2+} ions are released from the glass surface and H_3O^+ ions from the SBF solution are uptaken by the glass. This ionic exchange leads to the formation of silanol groups (Si-OH) at the glass surface according to the following reaction: $Si\text{-}O^- -- Ca^{2+} -- {}^-O\text{-}Si + 2\ H_3O^+ \rightarrow 2\ \text{-}Si\text{-}OH + Ca^{2+} + 2H_2O$ (Figure 7 - step 1). The decrease in H_3O^+ leads to an alkaline pH which is responsible for the continuous hydrolysis of Si-O-Si and formation of a soluble $Si(OH)_4$ which explains the increase of Si concentration after immersion (Figure 7 - step 2). The silanol groups at the glass surface condense to form a silica gel layer according to the reaction $\text{-}Si\text{-}OH + HO\text{-}Si\text{-} \rightarrow \text{-}Si\text{-}O\text{-}Si\text{-} + H_2O$. At this stage, Ca^{2+} and PO_4^{3-} ions precipitate on the silica gel layer surface from the SBF to form the carbonated apatite phase. This mechanism is in good agreement with the simultaneous decrease in SBF concentrations of Ca and P recorded by ICP-OES between day 10 and day 15 for 92S6 (Figure 4.A) and from day 1 for 92S6 P123 (Figure 4.B). These decreases are due to the migration of Ca^{2+} and PO_4^{3-} from the SBF towards the glass surface to form at first an amorphous apatite layer on the silica gel layer (Figure 7 - step 3) which after incorporating OH^- and CO_3^{2-} from SBF crystallizes in hydroxyl-carbonate apatite (HCA) (Figure 7 - step 4) after 1 day of immersion on 92S6 P123 surface and 15 days of immersion on 92S6 surface. This phenomenon explains the characteristic bands and peaks of HCA recorded in both FTIR-spectroscopy and XRD analysis respectively.

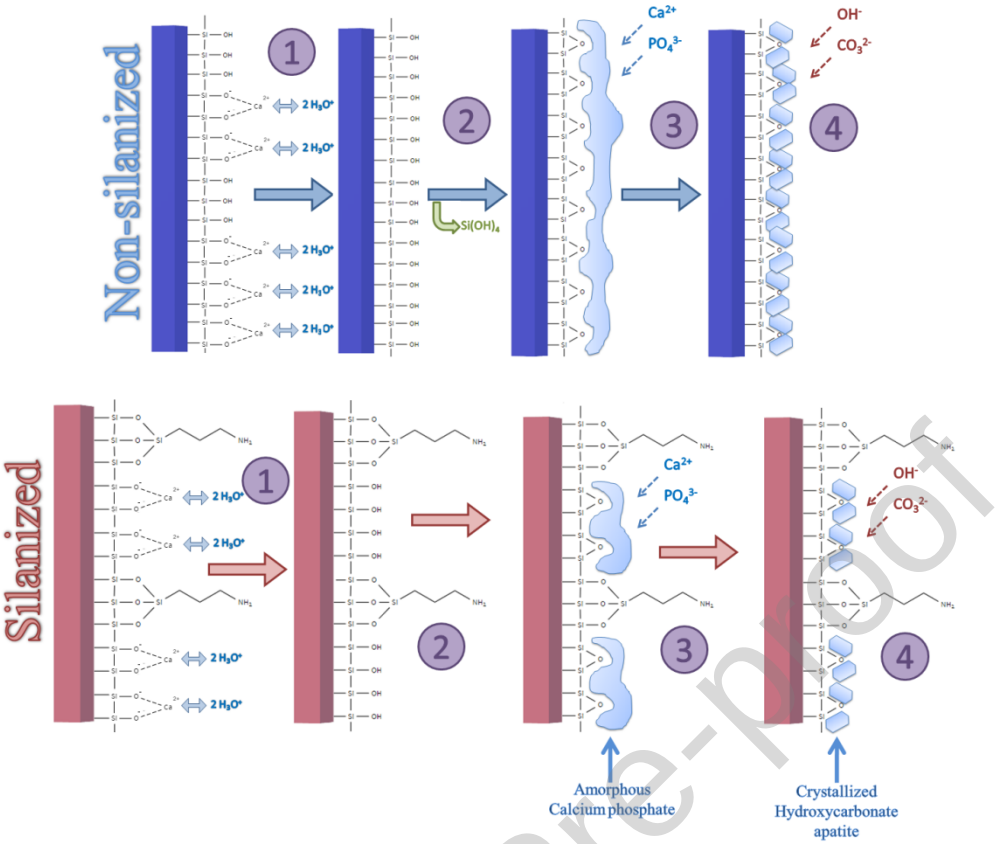

Figure 7. Reactions sequence between bioactive glass and SBF.

The XRD patterns and FTIR spectra show a faster formation of HCA on 92S6 P123 surface (after 1 day of immersion) in comparison with 92S6 where HCA is formed only after 15 days of immersion. The porosity patterning using pluronic P123 surfactant in the synthesis medium of 92S6 glass induces a regular, organized and well-defined structured porosity [18] (Figure 1.B), an increase of the specific surface area from 372 m^2/g to 392 m^2/g and a greater average pore diameter with a lower dispersion of pores diameter compared to 92S6 synthesized without any surfactant (Figure 1.A). The structured porosity leads to a greater and easier contact with SBF by an easy diffusion and then a higher reactivity of the glass towards SBF [14]. Consequently, it allows a rapid availability of high concentration of Ca^{2+} in the medium which precipitates afterwards with PO_4^{3-} to form HCA [45].

The ICP-OES analyses confirm the XRD analysis and FTIR-spectroscopy results and show that the kinetic of ionic exchange and the formation of the hydroxyl-carbonate apatite layer is faster for 92S6 P123 than for 92S6. After one day of soaking, the increase in Ca concentration recorded for 92S6 was not observed for 92S6 P123. This fact is consistent with the absence of formation of apatite layer consecutive to the calcium ions released by the 92S6 glass surface. For 92S6 P123, no significant increase in Ca concentration was recorded one day after soaking: the calcium release was counterbalanced by the calcium uptake for the formation of the calcium phosphate phase: hydroxyl-carbonate apatite (HCA).

Additionally to the difference in the formation rate of HCA, related to the difference in porosity features between the two glasses, a significant difference is observed between the 92S6 and 92S6P123 (and their silanized counterparts) about the co-precipitation of calcium carbonate phase, calcite, at the glass surface. As mentioned before, no calcite peak has been recorded for structured glasses 92S6P123 (and 92S6 P123 Sil) despite the fact that it exhibits high reactivity in SBF. In a previous study, it was demonstrated that the formation of calcite on glass surface is related to the continuous release of the Ca^{2+} ions which, reaching a given concentration, combine with the CO_3^{2-} ions present in the SBF and then precipitate as calcite at the glass surface [35]. Clearly the results found in this study contradict this phenomenon for glasses with ordered porosity. Structured glasses should undergo *a priori* precipitation of calcite in a more obvious way than for unstructured glass, because of the higher contact surface with SBF. Surprisingly, this is not what the results showed. This lack of precipitation seems to be linked to the structure of the porosity that leads to a confined environment, and a well-determined spatial orientation. It is known that in addition to calcite, calcium carbonates can crystallize in other forms, namely aragonite and vaterite. The thermodynamic stability of these various forms, in the ambient aqueous conditions, is in according to descending order: calcite > aragonite > vaterite [46].

Zeng et *al.* demonstrated that the crystallization of calcium carbonates in one form or another depends closely on the architecture and volume of the medium in which the phenomenon occurs [47]. The results of their study showed that the more confined the medium, the more the calcium carbonates crystallize as aragonite instead of calcite. The absence of calcite precipitation at the 92S6P123 glass surface is likely due to the fact that the confined medium within the structured glass prevents the precipitation of calcite. The precipitation of the more soluble and less stable aragonite does not occur before the formation of the calcium phosphate phase and the increase in Ca^{2+}concentration allows calcium phosphate formation and crystallization of apatite instead of anarchic calcite precipitation in the early stages of immersion. For the 92S6 unstructured glass, we recorded an absence of HCA crystals up to day 15. Calcite precipitate on the first day of immersion and persists throughout the duration of immersion, this is at the origin of the very slow formation of the HCA, which occurs only on the 15th day of immersion.

3.8. Effect of silanization on glass bioactivity

Despite a decrease in specific surface area and in average pore diameter for silanized glasses, the porosity patterning of 92S6 P123 is preserved (Figure 1.C). On the other hand, the ICP-OES results, XRD patterns and FTIR spectra showed that the silanization of the glasses surface did not significantly affect the glasses reactivity towards SBF. This can be explained by the fact that the free silanol groups on the glass surface are not part of the interaction with SBF in terms of ionic exchange (Figure 7- step 1). Indeed, in the glass network, it is the network modifiers that initiate the ionic exchange with the SBF; in our case, the network modifier is the calcium ion. On the other hand, the silanization does not lead to an impervious surface and consequently does not affect the SBF infiltration in the glass matrix [48]. As described above, following the cationic exchange between Ca^{2+} and H_3O^+, silanol groups are formed and subsequently condense to form a silica gel layer on which HCA is formed. It is

also, worth mentioning that the absence of any difference in Si evolution in SBF between silanized and non-silanized glass show that the silane coupling agent is strongly fixed to the surface of the glass and this fixation is not altered by the ionic exchanges that occur between the glass and SBF.

The SEM-EDS results are consistent with FTIR-spectra, XRD patterns and ICP-OES results in terms of the faster growth of HCA on 92S6 P123 in comparison to 92S6 and also in the fact that surface silanization does not affect glass reactivity toward SBF.

Conclusion

In this work, we have demonstrated the significant impact of porosity structuring on *in vitro* bioactivity of 92S6 sol-gel derived glass. Indeed, the ordered shape of the porosity has increased the surface contact between SBF and the glass, which leads to an increase in the ionic exchange kinetics and, consequently, to a faster growth of HCA layer on the bioactive glass surface. We also highlighted the impact of porosity structuring on calcite formation instead of, or in competition with hydroxy-carbonate apatite, the results showed that porosity structuring leads to a confined medium that hinders the ability of calcium carbonate to crystallize as calcite and therefore the Ca^{2+} ions released from glass combine rapidly with PO_4^{3-} to form HCA. The results of this work showed that the porosity structuring of bioactive glass allows the control of crystallization of calcite and consequently the crystallization of HCA, this opens a path toward a deep exploration of this physicochemical phenomenon that allows modulating the reactivity of glass in the SBF, by controlling the crystallization of HCA as a function of textural features of the glass matrix.

On the other hand, we studied the effect of the glass surface silanization on bioactivity feature. We first show that the ordered porosity facilitates the silane grafting. Afterward, we showed that silanization of the glass surface did not impact its reactivity towards the SBF. Indeed, the functional groups on the glass surface involved in the silanization process are not involved in the cationic exchange that occurs after contact with the SBF solution and therefore the bioactivity of the glass remains intact. Results also indicate that the bond between glass and the silane coupling agent is stable despite ionic exchanges and formation of apatite layer. A chemically stable silanized surface will allow the grafting of therapeutic molecules and a very interesting delayed release of the grafted molecules useful in treating cancer and bacterial invasions. The obtained results showed that the surface silanization can only be beneficial to bioactive glass. This surface treatment method allows the bioactive glass to be biologically and/or therapeutically more active, or strengthens one or more of its physicochemical or biological properties without negatively impacting its bioactivity. Our glasses are envisaged as controlled release devices for therapeutic molecules through surface functionalization by silanization.

In conclusion, it should be noted that our sol-gel bioactive glasses 92S6, because of their moldable physicochemical and biological properties, by modulating their porosity and/or surface functionalization, make them good candidates as bioactive implants and drug carriers for bone applications.

Acknowledgments

The authors of this article would like to acknowledge Vincent Dorcet for the assistance in TEM experiments performed on the THEMIS platform (ScanMAT, UAR2025 University of Rennes 1-CNRS; CPER-FEDER 2007–2014), Loïc Joanny (CMEBA) for SEM-EDS analysis, and François Cheviré (ICSR, Laboratory "Glasses and Ceramics") for XRD analysis at the Université de Rennes 1.

References

[1] Hench, L.L., 1991. Bioceramics: From Concept to Clinic. Journal of the American Ceramic Society 74, 1487–1510. https://doi.org/10.1111/j.1151-2916.1991.tb07132.x

[2] Hench LL., 1998. Bioceramics, a clinical success. American Ceramic Society Bulletin 77, 67–74.

[3] Hench, L., Polak, J., 2002. Third-Generation Biomedical Materials. Science (New York, N.Y.) 295, 1014–1017. https://doi.org/10.1126/science.1067404

[4] Hench, L.L., 2006. The story of Bioglass. Journal of Materials Science. Materials in Medicine17, 967–978. https://doi.org/10.1007/s10856-006-0432-z

[5] Hench L. L, 1998. Bioceramics. Journal of the American Ceramic Society 81, 1705–1728.

[6] Hench, L.L., Splinter, R.J., Allen, W.C., Greenlee, T.K., 1971. Bonding mechanisms at the interface of ceramic prosthetic materials. Journal of Biomedical Materials Research 5, 117–141. https://doi.org/10.1002/jbm.820050611

[7] Waltimo, T., Mohn, D., Paqué, F., Brunner, T.J., Stark, W.J., Imfeld, T., Schätzle, M., Zehnder, M., 2009. Fine-tuning of bioactive glass for root canal disinfection. Journal of Dental Research 88, 235–238. https://doi.org/10.1177/0022034508330315

[8] Ducheyne, P., 1985. Bioglass coatings and bioglass composites as implant materials. Journal of Biomedical Materials Research 19, 273–291. https://doi.org/10.1002/jbm.820190309

[9] Kitsugi, T., Nakamura, T., Oka, M., Senaha, Y., Goto, T., Shibuya, T., 1996. Bone-bonding behavior of plasma-sprayed coatings of BioglassR, AW-glass ceramic, and tricalcium phosphate on titanium alloy. Journal of Biomedical Materials Research 30, 261–269. https://doi.org/10.1002/(SICI)1097-4636(199602)30:2<261::AID-JBM17>3.0.CO;2-P

[10] Stöber, W., Fink, A., Bohn, E., 1968. Controlled growth of monodisperse silica spheres in the micron size range. Journal of Colloid and Interface Science 26, 62–69. https://doi.org/10.1016/0021-9797(68)90272-5

[11] Mezahi, F.-Z., Lucas-Girot, A., Oudadesse, H., Harabi, A., 2013. Reactivity kinetics of 52S4 glass in the quaternary system SiO_2–CaO–Na_2O–P_2O_5: Influence of the synthesis process: Melting versus sol–gel. Journal of Non-Crystalline Solids 361, 111–118. https://doi.org/10.1016/j.jnoncrysol.2012.10.013

[12] Lin, S., Ionescu, C., Pike, K.J., Smith, M.E., Jones, J.R., 2009. Nanostructure evolution and calcium distribution in sol–gel derived bioactive glass. Journal of Materials Chemistry. 19, 1276–1282. https://doi.org/10.1039/B814292K

[13] Sepulveda, P., Jones, J.R., Hench, L.L., 2001. Characterization of melt-derived 45S5 and sol-gel-derived 58S bioactive glasses. Journal of Biomedical Materials Research 58, 734–740. https://doi.org/10.1002/jbm.10026

[14] Migneco, C., Fiume, E., Verné, E., Baino, F., 2020. A Guided Walk through the World of Mesoporous Bioactive Glasses (MBGs): Fundamentals, Processing, and Applications. Nanomaterials 10, 2571. https://doi.org/10.3390/nano10122571

[15]Mabrouk, M., Mostafa, A., Oudadesse, H., Wers, E., Lucas-Girot, A., El-Gohary, M.I., 2014. Comparative Study of Nanobioactive Glass Quaternary System 46S6. Bioceramics Development and Applications 4, 1. https://doi.org/10.4172/2090-5025.1000072

[16]Letaief, N., Lucas-Girot, A., Oudadesse, H., Dorbez-Sridi, R., 2014. Influence of Synthesis Parameters on the Structure, Pore Morphology and Bioactivity of a New Mesoporous Glass. Journal of Biosciences and Medicines 2, 57–63. https://doi.org/10.4236/jbm.2014.22009

[17]Letaïef, N., Lucas-Girot, A., Oudadesse, H., Meleard, P., Pott, T., Jelassi, J., Dorbez-Sridi, R., 2014. Effect of aging temperature on the structure, pore morphology and bioactivity of new sol–gel synthesized bioglass. Journal of Non-Crystalline Solids 402, 194–199. https://doi.org/10.1016/j.jnoncrysol.2014.06.005

[18] Letaïef, N., Lucas-Girot, A., Oudadesse, H., Dorbez-Sridi, R., Boullay, P., 2014. Investigation of the surfactant type effect on characteristics and bioactivity of new mesoporous bioactive glass in the ternary system SiO_2–CaO–P_2O_5: Structural, textural and reactivity studies. Microporous and Mesoporous Materials 195, 102–111. https://doi.org/10.1016/j.micromeso.2014.03.035

[19]Letaïef, N., Lucas-Girot, A., Oudadesse, H., Dorbez-Sridi, R., 2014. New 92S6 mesoporous glass: Influence of surfactant carbon chain length on the structure, pore morphology and bioactivity. Materials Research Bulletin 60, 882–889.https://doi.org/10.1016/j.materresbull.2014.08.048

[20] Rocton, N., Oudadesse, H., Mosbahi, S., Bunetel, L., Pellen-Mussi, P., Lefeuvre, B., 2019. Study of nano bioactive glass for use as bone biomaterial comparison with micro bioactive glass behaviour. IOP Conference Series: Materials Science and Engineering 628, 012005. https://doi.org/10.1088/1757-899X/628/1/012005

[21]Dietrich, E., Oudadesse, H., Lucas-Girot, A., Le Gal, Y., Jeanne, S., Cathelineau, G., 2008. Effects of Mg and Zn on the Surface of Doped Melt-Derived Glass for Biomaterials Applications. Applied Surface Science255, 391–395. https://doi.org/10.1016/j.apsusc.2008.06.094

[22]Saravanapavan, P., Jones, J.R., Pryce, R.S., Hench, L.L., 2003. Bioactivity of gel-glass powders in the CaO-SiO_2 system: a comparison with ternary (CaO-P_2O_5-SiO_2) and quaternary glasses (SiO_2-CaO-P_2O_5-Na_2O). Journal of Biomedical Materials Research. Part A 66, 110–119. https://doi.org/10.1002/jbm.a.10532

[23]Ma, J., Chen, C.Z., Wang, D.G., Jiao, Y., Shi, J.Z., 2010. Effect of magnesia on the degradability and bioactivity of sol-gel derived SiO_2-CaO-MgO-P_2O_5 system glasses. Colloids and Surfaces. B, Biointerfaces 81, 87–95. https://doi.org/10.1016/j.colsurfb.2010.06.022

[24]Oudadesse, H., Dietrich, E., Gal, Y.L., Pellen, P., Bureau, B., Mostafa, A.A., Cathelineau, G., 2011. Apatite forming ability and cytocompatibility of pure and Zn-doped bioactive glasses. Biomedical Materials 6, 035006. https://doi.org/10.1088/1748-6041/6/3/035006

[25] Goel, A., Rajagopal, R.R., Ferreira, J.M.F., 2011. Influence of strontium on structure, sintering and biodegradation behaviour of CaO–MgO–SrO–SiO_2–P_2O_5–CaF_2 glasses. ActaBiomaterialia 7, 4071–4080. https://doi.org/10.1016/j.actbio.2011.06.047

[26] Yan, X., Yu, C., Zhou, X., Tang, J., Zhao, D., 2004. Highly ordered mesoporous bioactive glasses with superior in vitro bone-forming bioactivities. AngewandteChemie (International Ed. in English)43, 5980–5984. https://doi.org/10.1002/anie.200460598

[27] a) López-Noriega, A., Arcos, D., Izquierdo-Barba, I., Sakamoto, Y., Terasaki, O., Vallet-Regí, M., 2006. Ordered Mesoporous Bioactive Glasses for Bone Tissue Regeneration. Chemistry of Materials 18, 3137–3144. https://doi.org/10.1021/cm060488o

b) Shi, Q.H., Wang, J.F., Zhang, J.P., Fan, J., Stucky, G.D., 2006. Rapid-Setting, Mesoporous, Bioactive Glass Cements that Induce Accelerated In Vitro Apatite Formation. Advanced Materials 18, 1038–1042. https://doi.org/10.1002/adma.200502292

c) Izquierdo-Barba, I., Arcos, D., Sakamoto, Y., Terasaki, O., López-Noriega, A., Vallet-Regí, M., 2008. High-Performance Mesoporous Bioceramics Mimicking Bone Mineralization. Chemistry of Materials 20, 3191–3198. https://doi.org/10.1021/cm800172x

d) Ostomel, T.A., Shi, Q., Tsung, C.-K., Liang, H., Stucky, G.D., 2006. Spherical bioactive glass with enhanced rates of hydroxyapatite deposition and hemostatic activity. Small 2, 1261–1265. https://doi.org/10.1002/smll.200600177

e) Sun, J., Li, Y., Li, Liang, Zhao, W., Li, Lei, Gao, J., Ruan, M., Shi, J., 2008. Functionalization and bioactivity in vitro of mesoporous bioactive glasses. Journal of Non-Crystalline Solids 354, 3799–3805. https://doi.org/10.1016/j.jnoncrysol.2008.05.001

f) Yun, H., Kim, S., Hyun, Y., 2008. Preparation of 3D cubic ordered mesoporous bioactive glasses. Solid State Sciences 10, 1083–1092. https://doi.org/10.1016/j.solidstatesciences.2007.11.037

g) Yun, H., Kim, S., Hyeon, Y., 2007. Highly ordered mesoporous bioactive glasses with Im3m symmetry. Materials Letters 23–24, 4569–4572. https://doi.org/10.1016/j.matlet.2007.02.075

[28]López-Noriega, A., Arcos, D., Vallet-Regí, M., 2010. Functionalizing mesoporous bioglasses for long-term anti-osteoporotic drug delivery. Chemistry 16, 10879–10886. https://doi.org/10.1002/chem.201000137

[29]Gupta, N., Santhiya, D., Murugavel, S., Kumar, A., Aditya, A., Ganguli, M., Gupta, S., 2018. Effects of transition metal ion dopants (Ag, Cu and Fe) on the structural, mechanical and antibacterial properties of bioactive glass. Colloids and Surfaces A: Physicochemical and Engineering Aspects 538, 393–403. https://doi.org/10.1016/j.colsurfa.2017.11.023

[30]Colilla, M., Vallet-Regí, M., 2017. Ordered Mesoporous Silica Materials, in: Comprehensive Biomaterials II. pp. 644–685. Amsterdam, Netherlands: Elsevier, 2017. https://doi.org/10.1016/b978-0-12-803581-8.10231-0

[31] Majors, R.E., Hopper, M.J., 1974. Studies of Siloxane Phases Bonded to Silica Gel for Use in High Performance Liquid Chromatography. Journal of Chromatographic Science 12, 767–778. https://doi.org/10.1093/chromsci/12.12.767

[32]Kokubo, T., Kushitani, H., Sakka, S., Kitsugi, T., Yamamuro, T., 1990. Solutions able to reproduce in vivo surface-structure changes in bioactive glass-ceramic A-W. Journal of Biomedical Materials Research24, 721–734. https://doi.org/10.1002/jbm.820240607

[33]Kokubo, T., Takadama, H., 2006. How useful is SBF in predicting in vivo bone bioactivity? Biomaterials 27, 2907–2915. https://doi.org/10.1016/j.biomaterials.2006.01.017

[34] Bauer, F., Bilz, E., Chen, W.H., Freyer, A., Sauerland, V., Liu, S.B., 2007. Isomerization of n-butene over pre-coked HZSM-5 and HFER, in: Xu, R., Gao, Z., Chen, J., Yan, W. (Eds.), Studies in Surface Science and Catalysis, From Zeolites to Porous MOF Materials - The 40th Anniversary of International Zeolite Conference. Elsevier, 1096–1103. https://doi.org/10.1016/S0167-2991(07)80965-7

[35]Mami, M., Lucas-Girot, A., Oudadesse, H., Rachida, D.-S., Mezahi, F.-Z., Dietrich, E., 2008. Investigation of the Surface Reactivity of a Sol–Gel Derived Glass in the Ternary System SiO_2–CaO–P_2O_5. Applied Surface Science 254, 7386–7393. https://doi.org/10.1016/j.apsusc.2008.05.340

[36] Ashok, M., Sundaram, N.M., Kalkura, S.N., n.d, 2003. Crystallization of hydroxyapatite at physiological temperature. Materials Letters 57, 2066–2070.

[37]Indrani, D., Soegijono, B., Adi, W., Trout, N., 2018. Phase composition and crystallinity of hydroxyapatite with various heat treatment temperatures. International Journal of Applied Pharmaceutics 9, 87. https://doi.org/10.22159/ijap.2017.v9s2.21

[38]Doat, A., Pellé, F., Gardant, N., Lebugle, A., 2004. Synthesis of luminescent bioapatite nanoparticles for utilization as a biological probe. Journal of Solid State Chemistry 4–5, 1179–1187. https://doi.org/10.1016/j.jssc.2003.10.023

[39]Koutsopoulos, S., 2002. Synthesis and characterization of hydroxyapatite crystals: A review study on the analytical methods. Journal of Biomedical Materials Research 62, 600–612. https://doi.org/10.1002/jbm.10280

[40] Fu, Q., Rahaman, M.N., Zhou, N., Huang, W., Wang, D., Zhang, L., Li, H., 2008. In Vitro Study on Different Cell Response to Spherical Hydroxyapatite Nanoparticles. Journal of Biomaterials Applications 23, 37–50. https://doi.org/10.1177/0885328207081350

[41] Li, S., Hu, S., Yan, Y., Wang, Y., 2007. Investigation of HAP nanoparticles absorbed by hepatoma cells in vitro. Journal of Wuhan University of Technology-Mater Sci Ed 22, 288–290. https://doi.org/10.1007/s11595-005-2288-3

[42]Ohtsuki, C., Kokubo, T., Yamamuro, T., 1992. Mechanism of apatite formation on CaOSiO2P2O5 glasses in a simulated body fluid. Journal of Non-Crystalline Solids 143, 84–92. https://doi.org/10.1016/S0022-3093(05)80556-3

[43]LeGeros, R.Z., 1991. Calcium phosphates in oral biology and medicine. Monographs in Oral Science 15, 1–201.

[44] Li, P., Ohtsuki, C., Kokubo, T., Nakanishi, K., Soga, N., Nakamura, T., Yamamuro, T., 1993. Process of formation of bone-like apatite layer on silica gel. Journal of Materials Science: Materials in Medicine 4, 127–131. https://doi.org/10.1007/BF00120381

[45] Martínez, A., Izquierdo-Barba, I., Vallet-Regí, M., 2000. Bioactivity of a $CaO{-}SiO_2$ Binary Glasses System. Chemistry of Materials 12, 3080–3088. https://doi.org/10.1021/cm001107o

[46] Plummer, L.N., Busenberg, E., 1982. The solubilities of calcite, aragonite and vaterite in CO_2-H_2O solutions between 0 and 90°C, and an evaluation of the aqueous model for the system $CaCO_3$-CO_2-H_2O. GeochimicaetCosmochimicaActa 46, 1011–1040. https://doi.org/10.1016/0016-7037(82)90056-4

[47] Zeng, M., Kim, Y.-Y., Anduix-Canto, C., Frontera, C., Laundy, D., Kapur, N., Christenson, H.K., Meldrum, F.C., 2018. Confinement generates single-crystal aragonite rods at room temperature. Proceedings of the National Academy of Sciences of the United States of America 115, 7670–7675. https://doi.org/10.1073/pnas.1718926115

[48] Chen, Q., Rezwan, K., Querez, V., Armitage, D., Nazhat, S., Jones, F., Boccaccini, A., 2007. Surface Functionalization of Bioglass((R))-Derived Porous Scaffolds. Actabiomaterialia 3, 551–562. https://doi.org/10.1016/j.actbio.2007.01.008

Declaration of interests

✓☐The authors declare that they have no known competing financial interests or personal relationships that could have appeared to influence the work reported in this paper.

☐The authors declare the following financial interests/personal relationships which may be considered as potential competing interests:

Graphical abstract: